Polym. Bull. (2012) 69:1073–1091
DOI 10.1007/s00289-012-0780-4

ORIGINAL PAPER

# Effect of SEBS on morphology, thermal, and mechanical properties of PP/organoclay nanocomposites

**Zina Vuluga · Denis Mihaela Panaitescu · Constantin Radovici · Cristian Nicolae · Michaela Doina Iorga**

Received: 16 August 2011 / Revised: 18 April 2012 / Accepted: 28 May 2012 /
Published online: 9 June 2012
© Springer-Verlag 2012

**Abstract** A simultaneously increase in stiffness and toughness is needed for improving polypropylene (PP) competitiveness in automotive industry. The aim of this paper is to investigate the effects of styrene-(ethylene-*co*-butylene)-styrene triblock copolymer (SEBS) on mechanical and thermal properties of PP, in the presence and the absence of nanoclay. The amount of SEBS in PP was ranged to obtain the matrix with the most favorable stiffness–toughness balance. For this purpose, SEBS domain size and distribution in PP/SEBS blends was determined by means of atomic force microscopy and correlated with mechanical properties. The influence of SEBS on the crystalline structure of PP in PP/organoclay nanocomposites was investigated by X-ray diffraction and differential scanning calorimetry, a synergistic effect of SEBS and nanoclay being pointed out. Moreover large improvement in the impact strength (almost 22 times) was obtained in the case of SEBS-containing nanocomposite in comparison with the composite without SEBS.

**Keywords** PP nanocomposites · Mechanical properties · Stiffness–toughness balance · AFM

## Introduction

Polypropylene (PP) is considered one of the most promising substitutes for engineering materials in the automotive, construction, and electrotechnical industries

Z. Vuluga · D. M. Panaitescu (✉) · C. Nicolae · M. D. Iorga
Department of Polymer, National Institute for Research and Development in Chemistry and Petrochemistry, 202 Spl. Independentei, 060021 Bucharest, Romania
e-mail: panaitescu@icf.ro

C. Radovici
Department of Analysis, National Institute for Research and Development in Chemistry and Petrochemistry, 202 Spl. Independentei, 060021 Bucharest, Romania

because of its excellent processability, rigidity, thermal stability, resistance to oil, recyclability, and relatively low cost [1–5]. To improve PP competitiveness in engineering applications, a simultaneously increase in stiffness and toughness is necessary. Toughness, a very important mechanical property that reflects the material capacity to absorb the impact energy, can be considerably enhanced by the incorporation of a dispersed rubbery phase. Melt blending with rubbery materials such as ethylene–propylene copolymers, ethylene–propylene–diene monomer, butadiene–styrene–acrylonitrile terpolymers, acrylonitrile–butadiene rubber, styrene–butadiene–styrene copolymers or ethylene–octene copolymers, was extensively studied to improve PP impact strength [5–15]. Several studies related to PP–poly[styrene-(ethylene-*co*-butylene)-styrene] triblock copolymer (SEBS) blends were also reported [16–20]. For instance, a sharp brittle–tough transition was observed in the case of isotactic polypropylene (iPP) blended with 15 wt% of SEBS [17]. An appreciable effect of the blend morphology and especially, of the particle size of the rubbery phase on the toughness of PP blends was pointed out. It was suggested that melt viscosity and mixing conditions are important factors affecting the morphology of PP toughened with rubbery materials. Bassani et al. [17] obtained the best toughness, that is an increase of the impact strength of 25 times in relation to pure PP at 20 wt% SEBS in the blend, when a lower temperature profile of the extruder, a higher rotor speed, and a higher feed rate were used as processing conditions.

The incorporation of different fillers is a widely used method to enhance PP stiffness. The fillers effectiveness depends on many factors, the most important being the filler particle size and shape, and also the content and surface treatment of the filler [21]. Synthetic and mineral fillers such as talc, glass fibers, mica, glass beads, and calcium carbonate as well as wood flour and natural fibers were used to reinforce PP [22–25]. The replacement of conventional fillers with nano-fillers gave a new impulse to this field. Carbon nanotubes [1, 4], layered silicates [2, 26], and nanoparticles (silica, graphite, and calcium carbonate) [27–29] were tested to improve mechanical properties of PP. Among these materials, PP-clay nanocomposites are the most attractive, especially for application in automotive parts and the most studied too [30–32]. The results emphasized the influence of nanofiller dispersion into the matrix on mechanical properties of the composite and the difficulty to reach nano-level dispersion of fillers, usually hydrophilic materials, in highly hydrophobic matrices such as PP.

The reinforcing effect of layered silicate in PP/SEBS blends was far less investigated. Tjong et al. [33] investigated the effects of organoclay addition on the crystalline structure of the PP/SEBS–*g*–MA (maleated SEBS)/organoclay nanocomposites prepared by melt compounding. Analyzing XRD results at small angles, they obtained an enlarged interlayer distance, indicating an intercalation of PP and SEBS–*g*–MA molecular chains into the galleries of organoclay. They also obtained a doubling of the impact strength when small amounts of organoclay (2 %) were added in PP/20 %SEBS–MA composite, the increase being less important at higher amount of organoclay [33]. Su and Hang [34] studied PP/SEBS/organoclay nanocomposites, containing 15 wt% SEBS, prepared by melt compounding in a Brabender twin screw extruder. They tried to correlate macroscale properties, particularly mechanical properties, with the microstructure of PP/SEBS/organoclay

nanocomposites with the aim to achieve an optimum balance of impact strength and stiffness. They reported that the organoclay layers were mainly intercalated and partially exfoliated in nanocomposites, SEBS playing a more important role than PP because its polymer chains can easily intercalate the organoclay layers and expand the basal spacing. They formulated the hypothesis that the synergistic effect of both SEBS elastomer and organoclay nanoparticles should account for more balanced stiffness–toughness performance of the ternary nanocomposites.

This paper mainly aims to investigate the effects of SEBS on mechanical and thermal properties of PP, in the presence and the absence of nanoclay, in relation to the morphological characteristics. The amount of SEBS in PP was ranged to obtain the matrix with the most favorable stiffness–toughness balance for nanoclay composite preparation. The SEBS domain size in PP/SEBS blend was determined by means of atomic force microscopy (AFM) and correlated with the mechanical properties. The influence of SEBS on the crystalline structure of PP and PP/organoclay was investigated by X-ray diffraction (XRD) and differential scanning calorimetry (DSC). As a result, a larger improvement in the mechanical properties, and, especially in the impact strength in comparison with previously reported results, was obtained.

## Experimental part

### Materials

Polypropylene homopolymer Moplen HP400R (PP) produced by Bassel Polyolefins (Italy) with a MFI of 25 g/10 min (230 °C/2.16 kg) and a density of 0.900 g/cm$^3$ was used for blends and nanocomposites preparation. The impact modifier used in this research was a Kraton 1652 G (SEBS) from Kraton Polymers (USA), a linear poly[styrene-(ethylene-*co*-butylene)-styrene] block copolymer with a styrene content of 29 %, $M_n$ = 79,100, density of 0.91 g/cm$^3$, and MFI = 5.00 g/10 min (230 °C/5 kg). Dellite D67 (D67), an aluminum silicate organically modified with high content of ditallow dimethyl ammonium salt, was supplied by Laviosa Chimica Mineraria (Italy).

### Preparation of PP/SEBS blends

PP/SEBS blends (100/0, 86.5/13.5, 81.7/18.3, 77/23, and 70/30) were prepared by melt compounding in a DSE 20 Brabender Twin Screw Extruder. The temperatures of the extruder zones were 160, 165, 170, 175, 175, and 180 °C, respectively, and the rotational speed of the screws was 220 rpm. The speed of the feeding screws was maintained at 400 rpm. The extruded filaments were taken and granulated with a Brabender Pelletizer, the take-off speed being 12 m/min. Neat PP was extruded under similar conditions for comparison. Pelletized blends were dried in an oven for 4 h at 80 °C and standard tensile and impact strength specimens were prepared by injection molding. The conditions set to the injection molding machine (Engel 23/40) were for temperature 170, 180, and 190 °C, temperature of the mold being maintained at 50 °C. The obtained blends were named as PP, S1, S2, S3, and S4 for neat PP, PP with 13, 18, 23, and 30 wt% SEBS, respectively.

## Preparation of PP nanocomposites

PP/D67 nanocomposite was prepared by direct mixing PP with 10 wt% nanoclay D67 using a DSE 20 Brabender Twin Screw Extruder. Components were mixed for 30 min in a Turbula mixer prior to be fed in the extruder. The temperatures of the extruder zones were 160, 165, 170, 175, 175, and 180 °C, respectively, and the rotational speed of the screws was 220 rpm. The speed of the feeding screws was maintained at 280 rpm. PP/SEBS/D67 nanocomposite was prepared by a two step method. A masterbatch was first obtained from SEBS and 30 wt% nanoclay D67 on the twin screw extruder in the following conditions: temperature of the extruder zones was 160,165,170,165,175, and 165 °C, rotational speed of the screws was 220 rpm, the speed of the feeding screws was 280 rpm. The masterbatch was then diluted with PP granules until 10 wt% D67 in the composite on the same twin screw extruder in the conditions specified at PP/D67 nanocomposite preparation.

## Characterization

### *XRD*

XRD analyses of nanoclay, PP/SEBS blends and PP nanocomposites were performed on a DRON-UM X-ray diffractometer (horizontal goniometer–Bragg–Brentano geometry–reflexion) using CoK$\alpha$ radiation with $\lambda = 1.79021$ Å. The samples were scanned at a scanning rate of 0.02°/5 s from the $2\theta$ value of 1.5° to 12° and 0.05°/5 s from 12° to 37°. Samples were analyzed in reflection mode. The *d*-spacing (*d*) of the interlayer gallery of nanoclay and PP nanocomposites was calculated from the Bragg equation:

$$d = \lambda/(2\ \sin\theta_{\max}). \tag{1}$$

Specimens for XRD were taken from injection molded bars of 4 mm in thickness and a minimum surface of 20 × 20 mm.

### *Mechanical characterization*

Tensile properties of the composites were determined according to ISO 527 on specimens type IB (five specimens for each test) with 50 mm/min for the tensile strength and 2 mm/min for the modulus of elasticity, using an Instron 3382 Universal Testing Machine. According to ISO 527, the modulus of elasticity was determined from the slope of stress–strain curves between two strain values: 0.0005 and 0.0025 mm/mm, using the software of the Instron 3382, Bluehill 2 device. The tensile tests were performed in standard conditions of temperature and humidity: 25 °C and 50 % relative humidity.

### *Thermal characterization*

DSC was performed on a DSC Q2000 from TA Instruments under helium flow (100 ml/min). The samples weighing between 12 and 14 mg were cut from injection

molded specimens, packed in aluminum pans, and placed in the DSC cell. They were first heated from the ambient temperature to 200 °C to eliminate any previous thermal history and then cooled to the ambient temperature and heated again to 150 °C at a constant heating/cooling rate of 10 °C/min.

The degree of crystallinity $X_C$ was calculated from DSC curves as follows:

$$X_C = \frac{\Delta H}{\Delta H_o \, w_{PP}} \times 100 \quad (2)$$

where $\Delta H$ is the heat of fusion for the composite, $\Delta H_o$ is the heat of fusion for 100 % crystalline isotactic PP (190 J/g [35]), and $w_{PP}$ is the weight fraction of polymer matrix.

*Atomic Force Microscopy*

AFM images were captured in ScanAsyst mode by a MultiMode 8 atomic force microscope equipped with a Nanoscope V converter from Bruker (USA). ScanAsyst mode automatically optimizes imaging parameters including set-point, feedback gains, and scan rate to get an optimized image. Real-time scanning was performed in air at room temperature with scan rates of 0.7 Hz and scan angle 0°. A silicon tip (nominal radius 2 nm, from Bruker) with a cantilever length of 115 μm and a resonant frequency of about 70 kHz was used. The images (256 × 256) were recorded and analyzed using the AFM software NanoScope version 1.20.

## Results and discussion

XRD analysis

Figure 1 shows the diffraction patterns of neat PP and PP–SEBS blends with different amounts of block copolymer. The inter-planar distances, the integrated half width of the crystalline peaks ($\beta_{110}$, $\beta_{040}$, $\beta_{130}$, $\beta_{111}$, and $\beta_{041}$) proportional to the area of the peak divided by the height of the peak, and the crystallinity of PP matrix, ($I_C$) were calculated for all the samples and are presented in Tables 1 and 2 and in Fig. 2. The inter-planar distances ($d_{110}$, $d_{040}$, $d_{130}$, $d_{111}$, and $d_{041}$) were calculated using the Bragg's relationship. $I_C$ was calculated as a ratio between the areas under the crystalline peaks and the total area (under the crystalline and amorphous peaks) [36]. The measurement errors are ±0.1 % for inter-planar distances $d$, and ±0.5 % for $\beta_{ijk}$ integrated half width of the crystalline peaks. Although there are no significant changes in the crystalline structure of PP in the blends, as resulted from the analysis of the diffraction peaks, however, some modifications regarding the inter-planar distances and integrated half width of the crystalline peaks should be reported. A small increase of inter-planar distances, exceeding the experimental errors, can be signaled for samples with 13.5 and 18.3 wt% SEBS (S1 and S2), and, to a lesser extent, for samples S3 and S4, containing a larger amount of block copolymer (23 and 30 wt%). These increased $d$ values seem to indicate a penetration of block copolymer particles in the spherulite structure of PP.

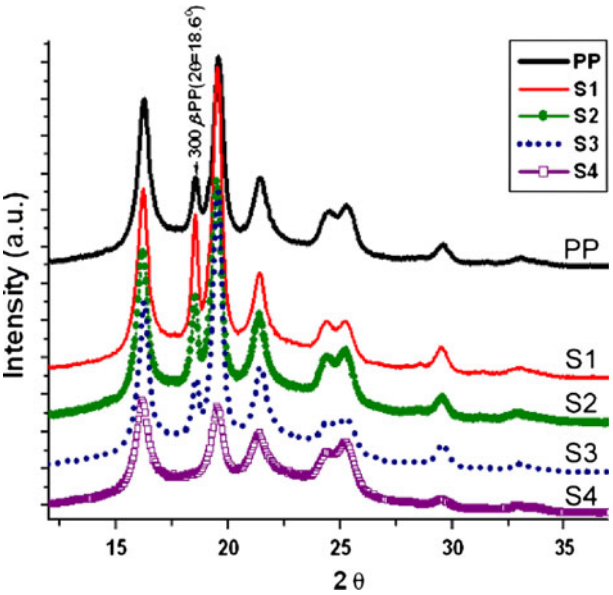


**Fig. 1** XRD patterns of neat PP and PP/SEBS blends

**Table 1** The inter-planar distances of neat PP, PP–SEBS blends, and PP nanocomposites

| Samples | $d_{110}$ (Å) | $d_{300}$ (Å) | $d_{040}$ (Å) | $d_{130}$ (Å) | $d_{111}$ (Å) | $d_{041}$ (Å) | $d_{060}$ (Å) | $d_{220}$ (Å) |
|---|---|---|---|---|---|---|---|---|
| PP | 6.331 | 5.552 | 5.271 | 4.803 | 4.221 | 4.081 | 3.504 | 3.150 |
| S1 | 6.352 | 5.558 | 5.286 | 4.815 | 4.233 | 4.092 | 3.512 | 3.158 |
| S2 | 6.359 | 5.566 | 5.284 | 4.818 | 4.231 | 4.091 | 3.509 | 3.160 |
| S3 | 6.338 | 5.553 | 5.278 | 4.806 | 4.229 | 4.087 | 3.507 | 3.153 |
| S4 | 6.348 | – | 5.277 | 4.815 | 4.228 | 4.089 | 3.507 | 3.158 |
| C0 | 6.321 | 5.537 | 5.270 | 4.797 | 4.218 | 4.077 | 3.504 | 3.152 |
| C | 6.335 | 5.544 | 5.277 | 4.804 | 4.177 | 4.066 | 3.507 | 3.141 |

**Table 2** Integrated half width of the crystalline peaks ($\beta_{110}$, $\beta_{040}$, $\beta_{130}$, $\beta_{111}$, and $\beta_{041}$) of neat PP, PP–SEBS blends, and PP nanocomposites

| Samples | $\beta_{110}$ (°) | $\beta_{300}$ (°) | $\beta_{040}$ (°) | $\beta_{130}$ (°) | $\beta_{111}$ (°) | $\beta_{041}$ (°) | $\beta_{060}$ (°) | $\beta_{220}$ (°) |
|---|---|---|---|---|---|---|---|---|
| PP | 0.751 | 0.393 | 0.578 | 0.784 | 0.987 | 0.950 | 0.754 | 0.987 |
| S1 | 0.716 | 0.363 | 0.535 | 0.686 | 0.912 | 0.883 | 0.701 | 0.986 |
| S2 | 0.720 | 0.384 | 0.579 | 0.765 | 0.925 | 0.903 | 0.719 | 0.934 |
| S3 | 0.708 | 0.366 | 0.549 | 0.708 | 0.921 | 0.930 | 0.717 | 0.944 |
| S4 | 0.842 | – | 0.628 | 0.863 | 0.950 | 0.984 | 0.711 | 0.881 |
| C0 | 0.675 | 0.410 | 0.514 | 0.616 | 0.838 | 0.810 | 0.695 | 1.196 |
| C | 0.684 | 0.396 | 0.515 | 0.611 | 1.139 | 0.598 | 0.684 | 0.933 |

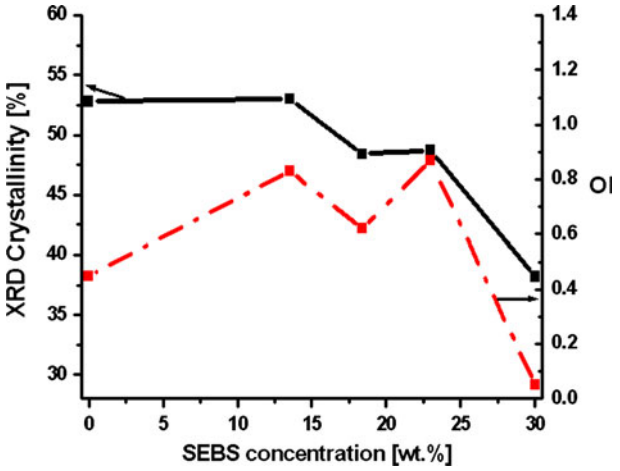


**Fig. 2** Variation in XRD crystallinity and orientation index (OI) with SEBS concentration in PP/SEBS blends

The decrease of the crystallinity noticed for PP–SEBS blends in comparison with neat PP (Fig. 2), was expected because of the influence of the elastomeric phase which hinders the crystallization process of PP, especially because of EB blocks interpenetrating the PP structure. However, the decrease of crystallinity is not proportional with the amount of SEBS in the blend, no change of crystallinity being observed for the smaller amount of SEBS (13.5 %). Likewise, smaller value was obtained for 18.3 wt% SEBS in the blend than for 23 wt% SEBS. These results could be due to the matching of the viscosities of the components in the melt processing step.

The $\beta$ and $\gamma$ crystalline phases of PP were identified from XRD patterns: the (300) diffraction peak at $2\theta = 18.6°$ is evidence for the presence of $\beta$ phase and the (117) diffraction peak at $2\theta = 22.4°$ is related to $\gamma$ phase. The position of these peaks was determined considering the wavelength $\lambda = 1.79021$ Å of Co K$\alpha$ radiation used in the test. The analysis of XRD diagrams shows that almost all the samples are mixtures of $\alpha$, $\beta$ and $\gamma$ PP. The intensity of the small diffraction peak at $2\theta = 18.60°$, ascribed to the $\beta$-form PP, is different from a sample to another (Fig. 1): it has the highest value for sample S1 and decreases in the order S1 > S2 > S3 > S4. This peak does not completely disappear in the case of S4 but it is very small and the determination of XRD parameters is difficult because of its very low intensity, to the limit of measurement errors. The increase of SEBS concentration seems to hinder the orientation of PP chains and the crystallization process. Moreover, between 23 and 30 % SEBS in the blend, a change of behavior is detected, probably influenced by the blend morphology. More information will be given by AFM investigations.

The relative amount of $\beta$-form was expressed as $K$ value [33] and was determined from the following equation (Table 3):

**Table 3** Relative amount of $\beta$-form PP, expressed as $K$ value, and the orientation index (OI) of neat PP, PP–SEBS blends, and PP nanocomposites

| Samples | $K$ | OI |
|---|---|---|
| PP | 7.34 | 0.45 |
| S1 | 12.48 | 0.83 |
| S2 | 10.54 | 0.62 |
| S3 | 6.62 | 0.87 |
| S4 | 0.00 | 0.05 |
| C0 | 4.39 | 2.00 |
| C | 4.18 | 1.52 |

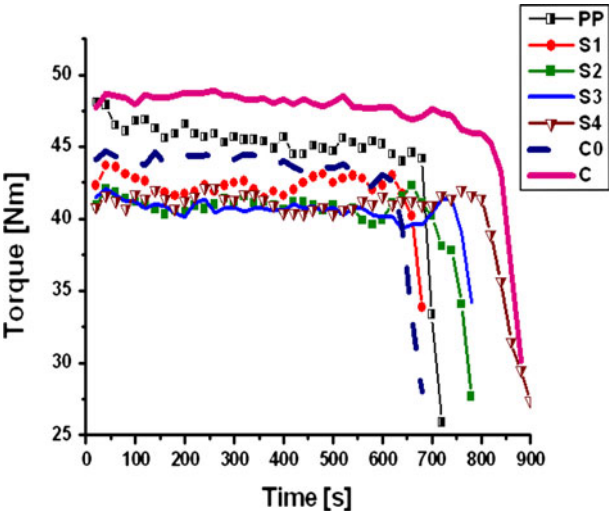


**Fig. 3** Torque–time curves for neat PP, PP/SEBS blends, and PP nanocomposites

$$K = \frac{A_\beta}{A_{110} + A_{040} + A_{130} + A_\beta} \tag{3}$$

where $A_\beta$ is the integrated area of the (300) diffraction peak of $\beta$-form PP, and $A_{110}$, $A_{040}$, and $A_{130}$ are the integrated area of (110), (040), and (130) diffraction peaks of the $\alpha$-form PP, respectively. The orientation index (OI), also shown in Table 3, was calculated from:

$$\mathrm{OI} = A_{040}/A_{110} - 0.55 \tag{4}$$

where 0.55 is the ratio of $A_{040}$ and $A_{110}$ determined for a perfect non-oriented PP. The change of orientation index of the samples with the concentration of SEBS in the blends (Fig. 2) shows some similarities with the crystallinity variation, a high increase of the OI being signaled for the samples with a higher crystallinity than expected (sample S3). There is no direct correlation between the concentration of SEBS and OI, which suggests the influence of other factors related to the behavior of blends during processing, the morphology of blends and the dispersion of SEBS

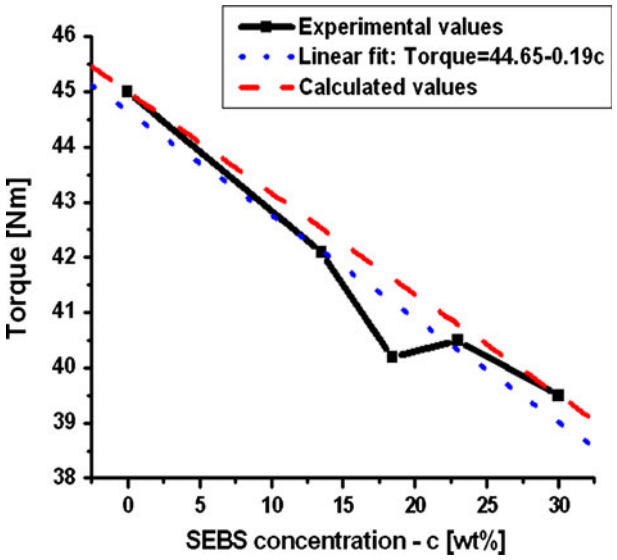


**Fig. 4** Variation in torque with SEBS concentration in PP/SEBS blends

in the matrix. The addition of SEBS in PP leads to higher values of OI, but at 30 % SEBS in the blend, a sharp decrease of OI is observed, which suggests a lower degree of SEBS dispersion in PP because of the aggregation of SEBS particles in bigger domains. AFM investigation could verify these observations. Regarding the behavior of blends during processing and its influence on the OI, the analysis of the melt viscosities of the blends could provide some explanation. The torque variation curves for the blends and composites during the melt process in the twin screw extruder are shown in Fig. 3. All the PP–SEBS blends show little variation of the torque during extrusion, a small decrease of at most 15 % of the initial value being detected at the end of the processing step. The variation of the torque after 10 min ($T$) depending on the concentration of SEBS in the blend ($c$) is not fully linear, as observed in Fig. 4, especially S2 torque value being far from the linear dependence expressed by $T = 44.65–0.19c$. The torque values of the blends S1, S2, and S3 are lower than the expected ones, taking into consideration the values for neat PP and for the PP blend with 30 %SEBS (sample S4), as shown in Fig. 4, indicating lower melt viscosities that favor orientation. Although, these results alone can not explain the different OI values obtained for these samples. Other influences could explain this behavior, for instance arising from the injection molding step.

From XRD patterns at small angle (Fig. 5) it can be noticed a different orientation of the quaternary ammonium salt between the silicate layers in D67, leading to disordered intercalated lamellar structures. D67 shows a disordered intercalated lamellar structure with at least three types of intercalates. Different interlamellar distances can be noticed: for $2\theta = 3.16^\circ$, $d = 32.7$ Å, $\beta = 1.02^\circ$, for $2\theta = 5.34^\circ$, $d = 19.1$ Å, $\beta = 1.69^\circ$, and for $2\theta = 8.40^\circ$, $d = 12.24$ Å, and $\beta = 0.96^\circ$. In PP composites containing SEBS and/or Dellite 67 it can be noticed

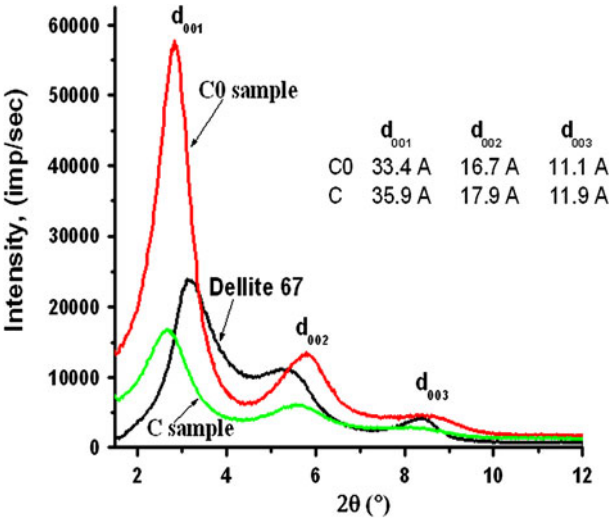


**Fig. 5** Small-angle XRD patterns of nanoclay (D67) and PP nanocomposites (C0 and C)

a rearrangement of the quaternary ammonium salt and homogeneous nanocomposites having ordered lamellar structure are obtained (Fig. 5). The basal spacing increases with about 3 Å (from about 33 Å in Dellite 67 to about 36 Å in composite based on PP, SEBS, and D67—sample C). The intensity of the characteristic peaks decreases, the peaks become broader, shift to lower angles, and the basal distance increases to 35.9 Å in PP/D67/SEBS. This behavior shows a good interaction of SEBS with D67. The good interaction between SEBS and D67 was also pointed out by Brabender torque results: sample C shows the highest melt viscosity from all the samples as indicated by torque value, although the melt viscosity of PP decreased with the addition of both SEBS and nanoclay.

Figure 6 shows the XRD patterns of PP/D67 (C0) and PP/SEBS/D67 (C) nanocomposites. No important differences regarding the crystalline structure of PP in nanocomposites can be observed in this figure and in Tables 2 and 3. Nevertheless, a decrease of $\beta_{ijk}$ integrated half widths for both nanocomposites, C and C0, as compared to neat PP and S3 must be noted in Table 2, indicating slightly higher crystallites size. Significantly higher OI values were found in PP nanocomposites as compared with PP and PP blends (Table 3), probably due to the nanoclay influence.

## Mechanical properties

Tensile stress–strain curves of PP/SEBS blends and PP nanocomposites are shown in Fig. 7. The incorporation of SEBS into PP leads to a significant increase of PP ductility as shown in this figure. The stress–strain curves of PP/SEBS blends exhibit the typical necking and neck propagation through the gauge length of the specimen, fracture occurring during the propagation of the neck or at the beginning of strain hardening. The addition of 13.5 wt% block copolymer in PP (S1) leads to a drastic decrease of the yield stress and a large increase of the elongation. Further addition

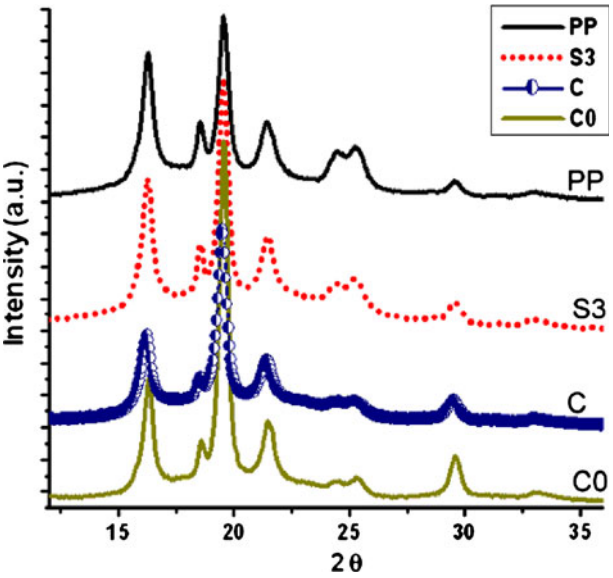


**Fig. 6** Diffraction patterns of neat PP and PP nanocomposites

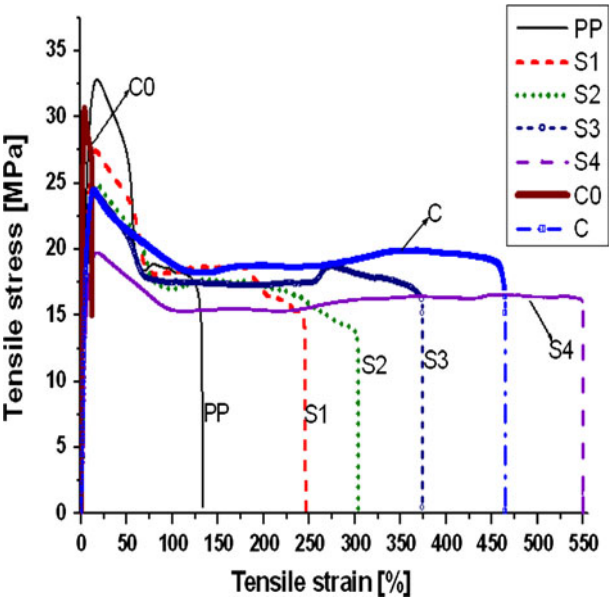


**Fig. 7** Tensile stress–strain curves of PP/SEBS blends and PP nanocomposites

of SEBS in PP leads to the decrease of the yield in different proportions but to a progressive increase of the elongation and energy at break, as can be seen in Fig. 8a, b. In these figures it can be also seen that the addition of SEBS leads to a decrease of

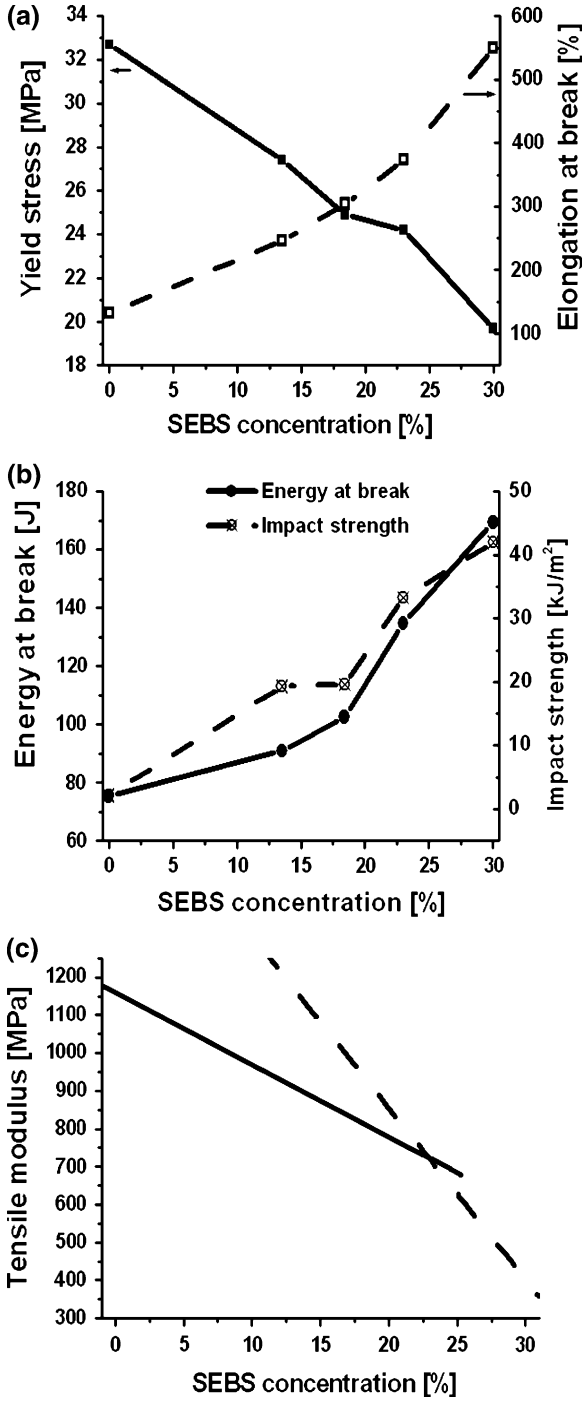


**Fig. 8** Mechanical properties of PP/SEBS blends depending on SEBS concentration: **a** yield stress and elongation at break. **b** Energy at break and impact strength. **c** Tensile modulus

**Table 4** Mechanical characteristics of PP nanocomposites

| Samples | Yield strength (MPa) | Axial strain at break (%) | Young's modulus of elasticity (MPa) | Energy at break (J) | Impact strength (KJ/m$^2$) |
|---|---|---|---|---|---|
| PP | 32.7 | 131.6 | 1160 | 75.4 | 2.2 |
| C0 | 30.0 | 35.8 | 1329 | 15.7 | 1.7 |
| S3 | 24.2 | 373.0 | 720 | 134.7 | 33.3 |
| C | 24.4 | 464.1 | 954 | 157.2 | 37.0 |

PP stiffness and an increase of toughness, the last one being expressed by the increase of both impact strength and energy at break values. Tensile modulus of PP/SEBS blends decreases almost linearly with the increase of block copolymer amount till ~23 wt% SEBS in the blend, after this concentration the decrease is more rapid (Fig. 8c). This could be a result of morphological changes in the blend. The characteristic feature of semi-plateau for the yield strength around 23 % block copolymer in the blend could indicate a higher strength of the interactions in this blend, since the yield stress is more sensitive to the interfacial interactions between the components of the blend as compared to tensile modulus.

It is known that SEBS is an effective impact modifier for PP. A spectacular increase of the impact strength is observed in Fig. 8b, the blend with 30 wt% SEBS (sample S4) showing an increase of 20 times of the impact strength as compared to neat PP. The increase is not linear and the deviations from linearity could be explained by the morphological features related to the elastomeric distribution, particle size, SEBS acting as a bumper that absorbs the impact energy and stops crack initiation.

The main mechanical characteristics of PP nanocomposites are given in Table 4. A slightly stiffening effect of the nanoclay can be noted when the characteristics of PP/D67 nanocomposite (sample C0) are compared to neat PP: tensile modulus is higher, yield and impact strength only slightly decrease, and elongation and energy at break are much lower. Similar variation of tensile modulus and impact strength was reported by Su and Huang in the case of PP/MA–PP/5 %clay nanocomposite [34]. The addition of 23 % SEBS in C0 nanocomposite results in a significant increase of elongation and energy at break (13 and 10 times, respectively). An increase of almost 22 times of the impact strength must be also noted. This remarkable increase of the material toughness seems to be a synergistic effect of nanoclay and SEBS.

## Thermal properties

Figure 9 shows the heating DSC termograms of PP and PP/SEBS blends in the temperature range in which melting of PP takes place. The melting temperatures of the blends ranges between 160.6 and 162.2 °C and are very close to that of neat PP, 161.3 °C. It must be noted that the smaller decrease of the melting temperature of sample S2 (PP with 18.3 % SEBS) is within experimental error (±0.5 °C) as well as the increased values observed in the case of S3 and S4 samples. With the exception of S3, the peaks widen for all the other blends as compared to neat PP. This could

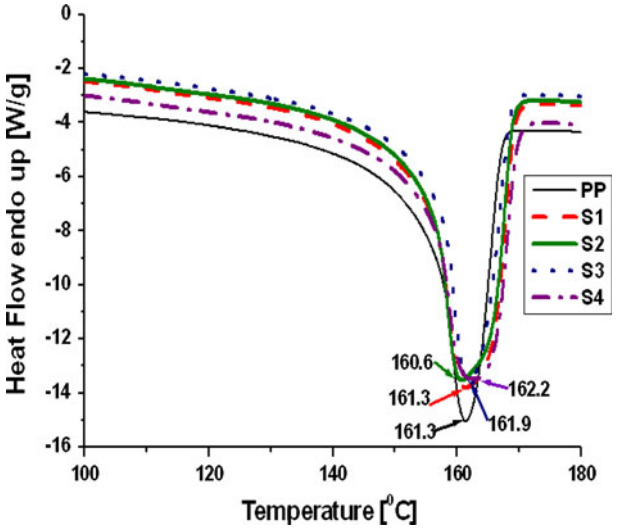


**Fig. 9** Heating DSC termograms of neat PP and PP/SEBS blends

indicate an increase of structural defects in crystalline PP phase in the blends. Some early studies reported a decrease of the melting point of PP with the increasing amount of SEBS in PP/SEBS/oil blends [37], explained by a reduction in the activity of the molten PP in the blends because of solubilization. However, Ferrer et al. [38] reported that the melting temperatures of PP/SBS blends with 0–90 % SBS were independent of blend composition and their value was 163 °C as in pure iPP, very close to our results. Different behaviors in terms of block copolymers influence on PP crystallinity determined from DSC thermograms have been reported in literature. Liao et al. [4] reported that PP blends with 15 and 30 wt% SEBS–MA prepared by melt compounding in a twin screw extruder showed an increase of the crystallinity up to 17 %, more obvious at lower concentration. Tjong et al. [33] obtained a decrease with 7 % of PP crystallinity when 15 wt% SEBS–MA was added, samples being prepared in similar facilities and working conditions in these both examples, except that in this second case, the mixture was once more processed to achieve more homogeneous blending. The crystallinity of our blends (Fig. 10) is lower than that of pure matrix, as previously reported by Tjong et al. [33], the decrease being not proportional with the SEBS content, as already observed in XRD analysis. Ohlsson et al. [9] reported that the crystallinity of PP was independent of composition in PP/SEBS/oil blends, where SEBS concentration ranged from 13.3 to 51.3 %. It is noteworthy that S3 sample (with 23 % SEBS) shows the highest crystallinity among PP/SEBS samples, in accordance with the XRD results. The highest OI and a higher XRD crystallinity than the expected values from the linear dependence were obtained for this sample. The PP crystallinity is one of the factors that influence the mechanical properties of the blends and the increased crystallinity observed in S3 sample is in good agreement with the increased values obtained for tensile modulus, impact strength and yield strength.

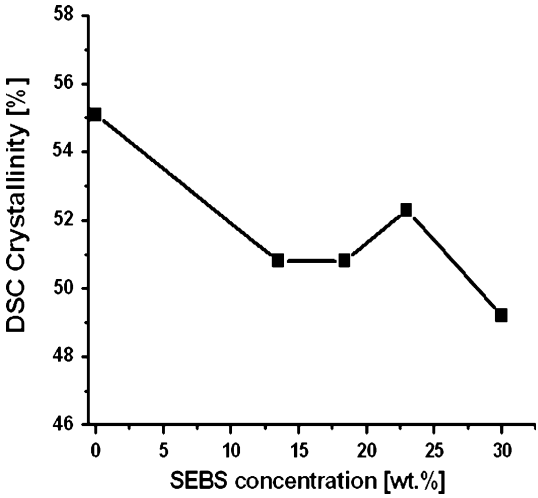


**Fig. 10** DSC crystallinity of PP/SEBS blends depending on SEBS concentration

Melting temperature ($T_m$), the temperature at the onset of melting curve ($T_{on}$), and the temperature at the completion of melting ($T_{mf}$), heat of fusion ($\Delta H_m$), and crystallinity ($I_C$) of PP nanocomposites as resulted from DSC thermograms are shown in Table 5. A slight increase of the melting temperature of PP is observed when nanoclay (C0) and both SEBS and nanoclay (C) are incorporated in PP. The increase of $T_m$, suggesting an increase in the overall lamellar size of PP, is in good agreement with XRD results that shown a decrease of $\beta_{ijk}$ integrated half widths for both nanocomposites, indicating slightly higher crystallites size. These features can be a result of better interaction at filler–matrix interface that prevents the molecular mobility of PP segments in the composites. Analyzing $T_{on}$ and $T_{mf}$ values, a widening of $T_{on}$–$T_{mf}$ was observed, from 13.8 °C for neat PP to 15.5 °C for PP/nanoclay and to 17.2 °C for the composite containing both SEBS and nanoclay. This widening suggests a broad size distribution of crystal lamellae. A decrease of nanocomposites crystallinity is observed as compared to neat PP, probably because the entanglement between SEBS and PP matrix and, possibly, the agglomerates of nanoparticles may hinder the lamellar alignment of the matrix. A slight decrease of PP crystallinity was also reported for different nanofillers added in PP [39]. The

**Table 5** Melting temperature ($T_m$), temperature at the onset of melting curve ($T_{on}$), temperature at the completion of melting ($T_{mf}$), heat of fusion ($\Delta H_m$), and crystallinity ($I_C$) of PP nanocomposites as resulted from DSC thermograms

| Samples | Temperature at the onset of melting curve $T_{on} \pm 0.3$ °C | Temperature at the completion of melting $T_{mf} \pm 0.3$ °C | Melting peak temperature $T_m \pm 0.3$ °C | Heat of fusion $\Delta H_m \pm 0.5$ % (J/g) | Crystallinity $I_C \pm 0.5$ % |
|---|---|---|---|---|---|
| PP | 155.4 | 169.2 | 161.3 | 104.7 | 55.1 |
| C0 | 155.9 | 171.4 | 162.7 | 82.8 | 52.1 |
| C | 153.9 | 171.1 | 164.4 | 63.8 | 50.1 |

lower fraction of crystals observed in nanocomposites as compared to neat PP is one of the factors that lead to a decrease of material strength. So, the slight decrease of crystallinity observed in DSC measurements for C0 and C, is in good agreement with the decrease of yield strength obtained by mechanical characterization.

Nevertheless, the information about the distribution of SEBS in PP can give new insights into the relation between mechanical and morphological features of these blends.

## Morphological investigation by AFM

The dispersion of SEBS in PP was analyzed by AFM. Phase images of PP/SEBS blends, scan area 2 × 2 μm$^2$, are shown in Fig. 11a–d. Different morphological features can be observed in PP/SEBS blends, considering that the darker areas represent the SEBS-rich domains. Some darker areas, rich in SEBS, with the size ranging from 100 nm to over 1 μm can be detected in S1 (PP/13 %SEBS—

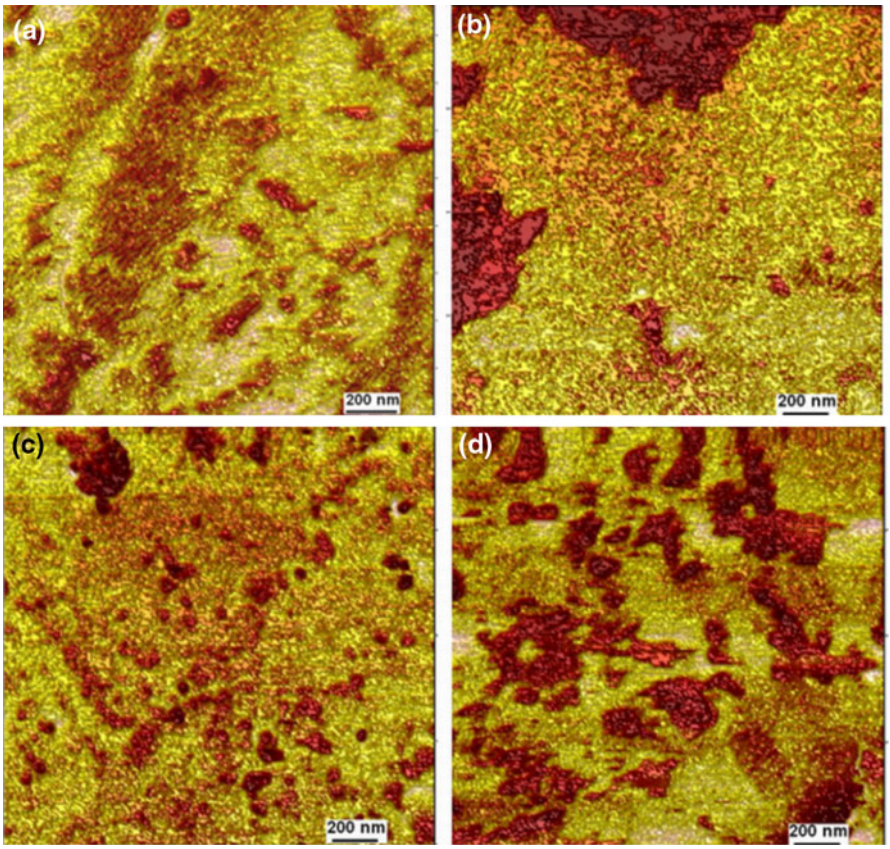


**Fig. 11** AFM phase images of PP/SEBS blends, scan area 2 × 2 μm$^2$: **a** S1 (PP/13 %SEBS). **b** S2 (PP/18 %SEBS). **c** S3(PP/23 %SEBS). **d** S4 (PP/30 %SEBS)

Fig. 11a). A characteristic of this blend is the nanometric dispersion of SEBS inside amorphous PP and the appearance of long-elongated areas rich in SEBS. Sample S2, with 18 % SEBS has a different aspect, large domains of more than one micron containing only SEBS, along with nanometric areas rich in SEBS are visible in Fig. 11b. This uneven dispersion of SEBS can explain the strong decrease of mechanical characteristics in the case of this blend (Fig. 8a, b). The best SEBS dispersion of all the samples can be observed in the case of S3 (Fig. 11c), which showed the highest crystallinity, orientation, and mechanical properties of all PP/SEBS analyzed blends. Thus, a direct relation between the OI value, crystallinity and size of SEBS domains can be observed. Larger, well-dispersed SEBS domains, most of them of approximately 500 nm can be detected in the case of S4 (PP/30 %SEBS blend—Fig. 11d). This dispersion of SEBS and the restrained PP area can explain both the higher ductility and toughness of this sample.

## Conclusions

The addition of SEBS in PP led to an important increase of toughness, as expressed by the increase of both impact strength and energy at break values. Tensile modulus of PP/SEBS blends decreased with the increase of block copolymer amount, from ~23 wt% SEBS in the blend the decrease being much more rapid. The highest ductility and toughness was obtained in the case of sample S4 (with 30 % SEBS), explained by the uniform dispersion of large SEBS domains, observed by AFM. The best stiffness–toughness balance was obtained in the case of sample S3 (PP/23 % SEBS), showing the highest OI, higher crystallinity (as determined by XRD and DSC), and small SEBS domains (most of them of 100–200 nm) homogenously dispersed in the matrix (as revealed by AFM images).

The addition of 23 % SEBS in a PP/nanoclay composite results in a significant increase of elongation and energy at break (13 and 10 times, respectively), and an increase of almost 22 times of the impact strength. The synergistic effect of nanoclay and SEBS, leading to this remarkable increase of the material toughness, was also supported by XRD results. From XRD patterns at small angle a decrease of the intensity of the characteristic peak and an expanded basal distance were observed in sample C, which contain both SEBS and D67. Moreover, the peaks became broader, shifted to lower angles and the basal distance increased, suggesting the intercalation of the SEBS between the silicate layers. The good interaction between SEBS and D67 was also pointed out by Brabender torque results: sample C showed the highest melt viscosity from all the samples as indicated by torque value, although the melt viscosity of PP decreased with the addition of only SEBS or nanoclay. The increased melting peak temperature of sample C as compared to C0 and neat PP, suggesting an increase in the overall lamellar size of PP, also supports the better interaction at filler–matrix interface in sample C, that prevents the molecular mobility of PP segments in this composite in comparison with the composite without SEBS.

The selection of the amount of SEBS based on the analysis of morphological features, thermal, and mechanical characteristics and the synergistic effect of SEBS

and organoclay led to a ternary PP/SEBS/nanoclay composite (C) with tailored characteristics for automotive industry.

**Acknowledgments** This study was supported by the 7th framework program of the European Union (Project NANOTOUGH FP7-NMP-2007-LARGE).

## References

1. Li C, Deng H, Wang K, Zhang Q, Chen F, Fu Q (2011) Strengthening and toughening of thermoplastic polyolefin elastomer using polypropylene-grafted multiwalled carbon nanotubes. J Appl Polym Sci 121:2104–2112
2. Hong CH, Lee YB, Bae JW, Jho JY, Nam BU, Hwang TW (2005) Preparation and mechanical properties of polypropylene/clay nanocomposites for automotive parts application. J Appl Polym Sci 98:427–433
3. Jahani Y (2011) Comparison of the effect of mica and talc and chemical coupling on the rheology, morphology, and mechanical properties of polypropylene composites. Polym Adv Technol 22: 942–950
4. Liao CZ, Tjong SC (2011) Effects of carbon nanofibers on the fracture, mechanical, and thermal properties of PP/SEBS–*g*–MA blends. Polym Eng Sci 51:948–958
5. Kobayashi Y, Otsuki Y, Kanai T (2010) Viscoelastic flow analysis of surface morphology on injection-molded polypropylene. Polym Eng Sci 50:2182–2189
6. Tortorella N, Beatty CL (2008) Morphology and mechanical properties of impact modified polypropylene blends. Polym Eng Sci 48:2098–2110
7. Bagheri H, Jahani Y, Haghighi MN, Hakim S, Fan ZQ (2011) Dynamic shear rheological behavior of PP/EPR in-reactor alloys synthesized by multi-stage sequential polymerization process. J Appl Polym Sci 120:3635–3641
8. Matsuda Y, Hara M (2005) Effect of the volume fraction of dispersed phase on toughness of injection molded polypropylene blended with SEBS, SEPS, and SEP. Polym Eng Sci 45:1630–1638
9. Ohlsson B, Hassander H, Tornell B (1996) Blends and thermoplastic interpenetrating polymer networks of polypropylene and polystyrene-block-poly(ethylene-*stat*-butylene)-block-polystyrene triblock copolymer 1. Morphology and structure-related properties. Polym Eng Sci 36:501–510
10. Matsuda Y, Hara M (2006) Effect of the compatibility on toughness of injection-molded polypropylene blended with EPR and SEBS. Polym Eng Sci 46:29–38
11. Ohlsson B, Tornell B (1998) Blends and interpenetrating polymer networks of polypropylene and polystyrene-block-poly(ethylene-*stat*-butylene)-block-polystyrene 2. Melt flow and injection molding properties. Polym Eng Sci 38:108–118
12. Jain AK, Nagpal AK, Singhal R, Gupta NK (2000) Effect of dynamic crosslinking on impact strength and other mechanical properties of polypropylene/ethylene-propylene-diene rubber blends. J Appl Polym Sci 78:2089–2103
13. Ha CS, Ray Chowdhury S, Kim GH, Kim I (2007) Polypropylene/ethylene–propylene–diene terpolymer blends. In: Nwabunma D, Kyu T (eds) Polyolefin blends. Wiley, New York, pp 411–440
14. Razavi-Nouri M, Naderi G, Parvin A, Ghoreishy MHR (2011) Thermal properties and morphology of isotactic polypropylene/acrylonitrile–butadiene rubber blends in the presence and absence of a nanoclay. J Appl Polym Sci 121:1365–1371
15. Liang JZ, Li RKY (2000) Rubber toughening in polypropylene: a review. J Appl Polym Sci 77:409–417
16. Stricker F, Thomann Y, Mulhaupt R (1998) Influence of rubber particle size on mechanical properties of polypropylene–SEBS blends. J Appl Polym Sci 68:1891–1901
17. Bassani A, Pessan LA, Hage E (2001) Toughening of polypropylene with styrene/ethylene-butylene/styrene tri-block copolymer: effects of mixing condition and elastomer content. J Appl Polym Sci 82:2185–2193
18. Bassani A, Pessan LA (2002) Toughening of polypropylene with styrene/ethylene-butylene/styrene tri-block copolymer: effects of reactive and nonreactive compatibilization. J Appl Polym Sci 86:3466–3479
19. Mae H, Omiya M, Kishimoto K (2008) Tensile behavior of polypropylene blended with bimodal distribution of styrene-ethylene-butadiene-styrene particle size. J Appl Polym Sci 107:3520–3528

20. Mae H, Omiya M, Kishimoto K (2008) Material ductility and toughening mechanism of polypropylene blended with bimodal distributed particle size of styrene–ethylene–butadiene–styrene triblock copolymer at high strain rate. J Appl Polym Sci 110:3941–3953
21. Kucera J, Nezbedova E (2007) Poly(propylene) with micro-fillers—the way of enhancement of toughness. Polym Adv Technol 18:112–116
22. Karian HG (2003) Handbook of polypropylene and polypropylene composites, revised and expanded. CRC Press, Boca Raton
23. Viksne A, Berzina R, Andersone I, Belkova L (2010) Study of plastic compounds containing polypropylene and wood derived fillers from waste of different origin. J Appl Polym Sci 117: 368–377
24. Mnif N, Massardier V, Kallel T, Elleuch B (2009) Study of the modification of the properties of (PP/EPR) blends with a view to preserving natural resources when elaborating new formulation and recycling polymers. Polym Compos 30:805–811
25. Eroglu M (2007) Effect of talc and heat treatment on the properties of polypropylene/EVA composite. Intern J Sci Techn 2:63–73
26. Pascual J, Fages E, Fenollar O, Garcıa D, Balart R (2009) Influence of the compatibilizer/nanoclay ratio on final properties of polypropylene matrix modified with montmorillonite-based organoclay. Polym Bull 62:367–380
27. Fu SY, Feng XQ, Lauke B, Mai YW (2008) Effects of particle size, particle/matrix interface adhesion and particle loading on mechanical properties of particulate–polymer composites. Compos Part B 39:933–961
28. Garces JM, Moll DJ, Bicerano J, Fibiger R, McLeod DG (2000) Polymeric nanocomposites for automotive applications. Adv Mater 12:1835–1839
29. Jipa S, Zaharescu T, Supaphol P (2010) Thermal stability of isotactic polypropylene modified with calcium carbonate nanoparticles. Polym Bull 64:783–790
30. Wang ZM, Nakajima H, Manias E, Chung TC (2003) Exfoliated PP/clay nanocomposites using ammonium-terminated PP as the organic modification for montmorillonite. Macromolecules 36: 8919–8922
31. Okamoto M, Nam PH, Maiti P, Kotaka T, Hasegawa N, Usuki A (2001) A house of cards structure in polypropylene/clay nanocomposites under elongational flow. Nano Lett 1:295–298
32. Palza H, Vergara R, Yazdani-Pedram M, Quijada R (2009) Polypropylene/clay nanocomposites: effect of different clays and compatibilizers on their morphology. J Appl Polym Sci 112:1278–1286
33. Tjong SC, Bao SP, Liang GD (2005) Polypropylene/montmorillonite nanocomposites toughened with SEBS–*g*–MA: structure–property relationship. J Polym Sci, Part B 43:3112–3126
34. Su FH, Huang HX (2009) Mechanical and rheological properties of PP/SEBS/OMMT ternary composites. J Appl Polym Sci 112:3016–3023
35. Panaitescu DM, Donescu D, Bercu C, Vuluga DM, Iorga MD, Ghiurea M (2007) Polymer composites with cellulose microfibrils. Polym Eng Sci 47:1128–1234
36. Ahmad Z, Kumar KD, Saroop M, Preschilla N, Biswas A, Bellare JR, Bhowmick AK (2010) Highly transparent thermoplastic elastomer from isotactic polypropylene and styrene/ethylene-butylene/styrene triblock copolymer: structure–property correlations. Polym Eng Sci 50:331–341
37. Ohlsson B, Tornell B (1996) Melt miscibility in blends of polypropylene, polystyrene-block-poly(ethylene-*stat*-butylene)-block-polystyrene and processing oil from melting point depression. Polym Eng Sci 36:1547–1556
38. Ferrer GG, Sanchez MS, Sanchez EV, Colomer FR, Ribelles JG (2000) Blends of styrene–butadiene–styrene triblock copolymer and isotactic polypropylene: morphology and thermomechanical properties. Polym Intern 49:853–859
39. Tarapow JA, Bernal CR, Alvarez VA (2009) Mechanical properties of polypropylene/clay nanocomposites: effect of clay content, polymer/clay compatibility, and processing conditions. J Appl Polym Sci 111:768–778